REPORT DOCUMENTATION PAGE

Public reporting burden for this collection of information is estimated to average 1 hour per response, including the time for reviewing instructions, searching existing data sources, gathering and maintaining the data needed, and completing and reviewing this collection of information. Send comments regarding this burden estimate or any other aspect of this collection of information, including suggestions for reducing this burden to Department of Defense, Washington Headquarters Services, Directorate for Information Operations and Reports (0704-0188), 1215 Jefferson Davis Highway, Suite 1204, Arlington, VA 22202-4302. Respondents should be aware that notwithstanding any other provision of law, no person shall be subject to any penalty for failing to comply with a collection of information if it does not display a currently valid OMB control number. **PLEASE DO NOT RETURN YOUR FORM TO THE ABOVE ADDRESS.**

1. REPORT DATE (DD-MM-YYYY) 15-09-2003	2. REPORT TYPE Journal Article	3. DATES COVERED (From - To) 2002

4. TITLE AND SUBTITLE
Effects of Classical and Quantum Charge Fluctuations on Sequential Electron Tunneling in Multiple Quantum Wells

5a. CONTRACT NUMBER

5b. GRANT NUMBER

5c. PROGRAM ELEMENT NUMBER
62601F

6. AUTHOR(S)
Danhong Huang and D.A. Cardimona

5d. PROJECT NUMBER
4846

5e. TASK NUMBER
CR

5f. WORK UNIT NUMBER
C1

7. PERFORMING ORGANIZATION NAME(S) AND ADDRESS(ES)
Air Force Research Laboratory
Space Vehicles Directorate
3550 Aberdeen Ave., SE
Kirtland AFB, NM 87117-5776

8. PERFORMING ORGANIZATION REPORT NUMBER

9. SPONSORING / MONITORING AGENCY NAME(S) AND ADDRESS(ES)

10. SPONSOR/MONITOR'S ACRONYM(S)

11. SPONSOR/MONITOR'S REPORT NUMBER(S)

12. DISTRIBUTION / AVAILABILITY STATEMENT
Approved for Public Release; Distribution is Unlimited.

13. SUPPLEMENTARY NOTES

14. ABSTRACT

A previous theory [M. Ershov *et al.*, Appl. Phys. Lett. **67**, 3147 (1995)] for studying the distribution of nonuniform fields in multiple-quantum-well photodetectors under an ac voltage is generalized to include nonadiabatic space-charge-field effects. From numerical results calculated by the generalized theory, it is found that field-domain effects are only important at high temperatures or high voltages, where both injection and sequential-tunneling currents are expected to be large. On the other hand, field-domain effects become negligible at low temperatures and low voltages, but nonadiabatic effects included in this extended theory are enhanced for small sequential-tunneling using the generalized theory, a differential capacitance is calculated for a non-steady state, and a negative conduction current is predicted under a positive voltage in this case due to charge accumulation around the collecting contact.

15. SUBJECT TERMS
Nonuniform fields, multiple quantum wells, nonadiabatic

16. SECURITY CLASSIFICATION OF:

a. REPORT	b. ABSTRACT	c. THIS PAGE	17. LIMITATION OF ABSTRACT	18. NUMBER OF PAGES	19a. NAME OF RESPONSIBLE PERSON Mr. David Cardimona
Unclassified	Unclassified	Unclassified	Unlimited	10	19b. TELEPHONE NUMBER (include area code) (505) 846-5807

Effects of classical and quantum charge fluctuations on sequential electron tunneling in multiple quantum wells

Danhong Huang[a] and D. A. Cardimona
Air Force Research Laboratory (AFRL/VSSS), Kirtland Air Force Base, New Mexico 87117

A previous theory [M. Ershov et al., Appl. Phys. Lett. **67**, 3147 (1995)] for studying the distribution of nonuniform fields in multiple-quantum-well photodetectors under an ac voltage is generalized to include nonadiabatic space-charge-field effects. From numerical results calculated by the generalized theory, it is found that field-domain effects are only important at high temperatures or high voltages, where both injection and sequential-tunneling currents are expected to be large. On the other hand, field-domain effects become negligible at low temperatures and low voltages, but nonadiabatic effects included in this extended theory are enhanced for small sequential-tunneling currents. The time duration for nonadiabatic effects is determined by the quantum capacitance. By using the generalized theory, a differential capacitance is calculated for a non-steady state, and a negative conduction current is predicted under a positive voltage in this case due to charge accumulation around the collecting contact.
[DOI: 10.1063/1.1594815]

I. INTRODUCTION

Multiple-quantum-well (MQW) photodetectors using intersubband transitions have attracted a lot of studies over the past few years.[1] Transient spectroscopy allows us to gain information on the sequential-tunneling processes between quantum wells (QWs) and thus QW parameters, including geometrical and QW capacitances at the same time.

When a voltage is applied to a MQW structure, electrons respond by producing a sequential-tunneling current. The interesting thing is that a uniform-field distribution inside the MQW structure is not stable if injection and sequential-tunneling currents are quite different from each other.[2] With the existence of an imbalance between injection and sequential-tunneling currents, the uniform electric field is split into many local fields. The local electric fields which are constant inside barrier layers are all different from each other, leading to a distribution of nonuniform electric fields within the MQW structure. The distribution of nonuniform fields depends on the applied voltage, and is accompanied by a nonuniform distribution of electron densities in different QWs. When the voltage varies with time, the distribution of nonuniform fields evolves with time, giving rise to varying field domains. The difference between two local electric fields within neighboring barrier layers is determined by the charge-density deviation from the equilibrium value inside the sandwiched QW through the boundary condition containing the quantum-well capacitance.

The MQW capacitance contains two parts. The first part is the geometrical capacitance which depends on the dielectric constant of the host semiconductors. The second part is the quantum capacitance which is attributed to the density-of-states of the two-dimensional electron gas in each QW. The geometrical capacitance is associated with classical charge fluctuations[2] after an ac voltage is applied. However, the quantum capacitance is related to the quantum charge fluctuations resulting from nonadiabatic space-charge-field effects.[3,4] The nonadiabatic nature of these effects is due to the fact that the transient currents that appear depend not only on the time-dependent electric field, but also on its time derivative.

Most of the previous calculations on the distribution of field domains were limited either to dc voltage[5] or to ac voltage in steady state. Very few calculations were done for ac voltage in non-steady state.[4] In steady state, charge fluctuations are adiabatic, namely the time derivatives of the charge densities in the QWs at each moment are zero. The detected conduction current equals the injection current which is modified by the local field at the emitter barrier. However, the time derivatives of the charge densities are no longer zero in non-steady-state conditions. In this case, charge might be dynamically accumulated or depleted in the MQWs. Adiabatic charge fluctuations only depend on the instantaneous voltage at each moment, while nonadiabatic charge fluctuations depend on both the voltage and its time derivative.

When the sequential-tunneling current is low, the impurity or defect channels within the barrier will play a role.[6] However, this only modifies the resistance of the sample for the sequential tunneling of electrons. The nonadiabatic effects discussed in this article for electron tunneling remain the same. For the same reason, the variation in barrier width and alloy composition will not affect nonadiabatic effects discussed in this article. Moreover, the self-consistent Hartree model with nonadiabatic effects on non-steady-state electrons under an ac electric field in multiple quantum wells has proven that the nonadiabatic effect discussed in this work is related to a shaking of the Fermi level in the nonequilibrium distribution function of electrons.[7]

---

[a]Electronic mail: danhong.huangd@kirtland.af.mil

The adiabatic field-domain theory[2,5] has been proven to be a great success to explain the quantitative difference between the experimental and uniform-field theoretical results at $T=77$ K and high voltages. On the other hand, the nonadiabatic tunneling model[4] under a uniform electric field has also been demonstrated successfully in explaining the experimentally found residual current[3] at zero ac voltage and $T=40$ K. Therefore it is quite reasonable to expect that the combination of these two theories will provide a complete description for electron sequential tunneling in MQWs at temperatures either above 77 K or below 40 K. It has been found that the nonadiabatic behavior (nonzero residual current) observed in transient tunneling currents as a function of bias voltage[3] can not be simply explained by Levine's adiabatic sequential-tunneling model[1] even after the field-domain effect[2] has been included. Therefore we require a nonadiabatic sequential-tunneling model with the inclusion of the field-domain effect to explain related experimental results in a wide range of temperatures. This is the motivation for this work.

In this article, we generalize the previous theory[2] for studying the distribution of nonuniform fields in MQW photodetectors under an ac voltage by including nonadiabatic space-charge-field effects. We find from numerical results that field-domain effects are only important at high temperatures or high voltages when both injection and sequential-tunneling currents are significant. On the other hand, we find that nonadiabatic effects included in the generalized theory become visible at low temperatures and low voltages when field-domain effects are negligible. The time duration for nonadiabatic effects is found to depend on the quantum capacitance, while the classical dielectric displacement current is found to be related to the geometrical capacitance. Moreover, a negative conduction current is predicted under a positive voltage in non-steady state. This article only discusses effects of classical and quantum charge fluctuations on the dark current in multiple-quantum-well photodetectors. However, these effects on photocurrent can be discussed in a similar way if we assume the tunneling current in this case to be the sum of the dark current and photocurrent.

The organization of the article is as follows. In Sec. II, we introduce our model for nonadiabatic charge-density fluctuations and the distribution of field domains in MQWs. Both classical and quantum charge fluctuations in QWs are formulated and studied. Numerical results and discussions are given in Sec. III for effects of classical and quantum charge fluctuations, including dependence on the total number of quantum wells N, temperature T, capture probability P_c, time period t_p, and amplitude $\mathcal{E}_0$ of an applied ac electric field, QW electron density n_{2D}, and contact-layer electron concentration n_c. The article is briefly concluded in Sec. IV with some remarks.

II. MODEL AND THEORY

In this section, we first study the effects of field domains resulting from the imbalance between injection and sequential-tunneling currents and show that these effects become negligible at low temperatures. After that, we general-
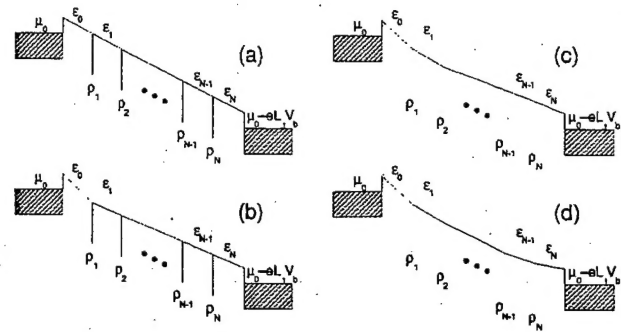

FIG. 1. The processes (a)–(d) for the formation of field domains in a multiple-quantum-well (MQW) sample with N quantum wells (QWs). Here, $\mathcal{E}_k$ for $k=0, 1, 2,...,N$ indicates local electric fields in $(N+1)$ different barrier layers, and ρ_k for $k=1, 2,...,N$ corresponds to different charge densities inside N QWs. μ_0 is the chemical potential in contact layers, V_b is the applied voltage, and L_t is the total length of MQWs.

ize the adiabatic field-domain theory by including nonadiabatic space-charge effects resulting from quantum capacitance.

A. Classical charge fluctuations

Electrons in QWs are confined in the direction perpendicular to the wells, while electrons in heavily doped contact layers are free in all three directions. Therefore we expect the tunneling of electrons from a contact layer to a QW (3D-to-2D) will be physically different from that of one QW to another (2D-to-2D).

As shown in Fig. 1, we see that the distribution of uniform dc electric fields in (a) with $\mathcal{E}_0=\mathcal{E}_1=\mathcal{E}_2=\cdots=\mathcal{E}_N$ is not stable if the injection current flowing from the left contact layer to the first QW and the sequential-tunneling current flowing from the first QW to the second QW are different.[2,5,8] As an example, we assume in Fig. 1(b) that the injection current is smaller than the sequential-tunneling current. In this situation, the local field $\mathcal{E}_0$ in the first barrier (emitter barrier) layer has to be increased so as to equalize these two currents. As a result of $\mathcal{E}_0>\mathcal{E}_1=\mathcal{E}_2=\cdots=\mathcal{E}_N$, we know from Maxwell equations that the charge density in the first QW will be reduced relative to the others,[5] i.e., $\rho_1<\rho_2=\rho_3=\cdots=\rho_N$. Now, let us further compare the tunneling currents flowing from the first QW to the second QW and that flowing from the second QW to the third QW. We realize from Fig. 1(c) that the tunneling current flowing from the first QW is less than that flowing from the second QW since $\rho_1<\rho_2$ for $\mathcal{E}_1=\mathcal{E}_2$. Therefore $\mathcal{E}_1>\mathcal{E}_2=\cdots=\mathcal{E}_N$ is required so as to equalize these two sequential tunneling currents. Consequently, we are left with $\rho_1<\rho_2<\rho_3=\cdots=\rho_N$. This process will continue up to the last (Nth) QW, as displayed in Fig. 1(d), until the initial field distribution $\mathcal{E}_0>\mathcal{E}_1>\mathcal{E}_2>\cdots>\mathcal{E}_N$ and density distribution $\rho_1<\rho_2<\rho_3<\cdots<\rho_N$ are reached. Here, the local field $\mathcal{E}_j(t)$ is a constant in the jth barrier layer, and the splitting of different local electric fields constructs the field domains in MQWs. The electric fields in different barrier regions in steady state will be redistributed if the total tunneling current flowing into the bottom contact layer is different from the injection current flowing out of the top contact layer. Therefore the above field-adjustment pro-

cess will be repeated again and again until the total tunneling current to the bottom contact layer is equal to the injection current from the top contact layer, and then, a stable distribution of local fields is formed. It should be noted that the distribution of electric-field domains in steady state depends on the value of voltage applied at each moment. A variation of the applied voltage with time results in varying field domains, and charge-density oscillations in each QW as well.

The injection current density (3D-to-2D) from the contact layer to the first QW is calculated to be[5]

$$
J_{\mathrm{inj}}^{3\mathrm{D}}[\mu_0, \mu_1(t), \mathcal{E}_0(t)]
$$

$$
= \left(\frac{e m^* k_B T}{2\pi^2 \hbar^3}\right)\left[\frac{\mathcal{E}_0(t)}{|\mathcal{E}_0(t)|}\right]\int_0^{+\infty} dE\, \mathcal{T}[E, |\mathcal{E}_0(t)|]
$$

$$
\times \ln\left\{\frac{1+\exp[(\mu_0-E)/k_B T]}{1+\exp\{[\mu_1(t)-E-eL_B|\mathcal{E}_0(t)|]/k_B T\}}\right\}, \qquad (1)
$$

where t is the time, m^* is the effective mass of electrons, T is the electron (or lattice) temperature, L_B is the thickness of the barrier, $\mathcal{T}[E, |\mathcal{E}(t)|]$ is the quantum transmission of electrons[6] with kinetic energy E through a barrier biased by an electric field $\mathcal{E}(t)$, and the chemical potential μ_0 in the contact layer is related to the electron concentration n_c by

$$
n_c = \frac{1}{2\pi^2}\left(\frac{2m^*}{\hbar^2}\right)^{3/2}\int_0^{+\infty} dE\, \sqrt{E}\left[1+\exp\left(\frac{E-\mu_0}{k_B T}\right)\right]^{-1}.
$$

For low T, electrons in QWs can only populate the ground subband with quantized energy E_0. Furthermore, the sequential-tunneling current density (2D-to-2D) from the kth QW to the neighboring $(k+1)$th QW is found to be[1]

$$
J_k^{2\mathrm{D}}[\mu_k(t), \mu_{k+1}(t), \mathcal{E}_k(t)]
$$

$$
= \left(\frac{e m^*}{\pi\hbar^2 L_W}\right) v_k^d[\mathcal{E}_k(t)]\int_0^{+\infty} dE\, \mathcal{T}[E+E_0, |\mathcal{E}_k(t)|]
$$

$$
\times \{f_0[E-\mu_k(t)] - f_0[E-\mu_{k+1}(t)+eL_B|\mathcal{E}_k(t)|]\},
$$

$$
(2)
$$

where L_W is the well width, $k=1, 2,\ldots,N$ represents the index of N wells, $\mathcal{E}_k(t)$ is the local electric field in the kth barrier region, $k=N+1$ corresponds to the bottom contact layer, $\mu_{N+1}=\mu_0$, $f_0(x)=[1+\exp(x/k_B T)]^{-1}$ is the Fermi–Dirac function, and the chemical potential $\mu_k(t)$ in the kth QW introduced in Eqs. (1) and (2) can be determined by the electron density $n_k(t)$ in the kth QW through

$$
\mu_k(t)=k_B T\ln\left\{\exp\left[\frac{\pi\hbar^2 n_k(t)}{m^* k_B T}\right]-1\right\},
$$

which is measured from E_0. In Eq. (2), $v_k^d[\mathcal{E}_k(t)]$ is the drift velocity of electrons in the kth barrier layer, given by[1]

$$
v_k^d[\mathcal{E}_k(t)] = \left[\frac{\mathcal{E}_k(t)}{\sqrt{\mathcal{E}_k^2(t)+\mathcal{E}_s^2}}\right] v_s,
$$

with the saturation velocity v_s and saturation field $\mathcal{E}_s$, respectively.

As explained in Fig. 1, the distribution of field domains changes with the value of the voltage $V_b(t)$ applied to the sample. When $V_b(t)$ varies with time, the field domain moves adiabatically across the whole sample, accompanied by the charge density that fluctuates in QWs. In this case, the propagation of the charge-density fluctuation $\rho_j(t)=en_j(t)$ can be described by the equation[2]

$$
\frac{d\rho_j(t)}{dt} = P_c\sum_{k=1}^{j-1}(1-P_c)^{j-k-1}J_k^{2\mathrm{D}}[\mu_k(t), \mu_{k+1}(t), \mathcal{E}_k(t)]\theta[\mathcal{E}_k(t)] + P_c(1-P_c)^{j-1}J_{\mathrm{inj}}^{3\mathrm{D}}[\mu_0, \mu_1(t), \mathcal{E}_0(t)]\theta[\mathcal{E}_0(t)]
$$

$$
- P_c\sum_{k=j+1}^{N}(1-P_c)^{k-j-1}J_k^{2\mathrm{D}}[\mu_k(t), \mu_{k-1}(t), \mathcal{E}_{k-1}(t)]\theta[-\mathcal{E}_{k-1}(t)] - P_c(1-P_c)^{N-j}J_{\mathrm{inj}}^{3\mathrm{D}}[\mu_0, \mu_N(t), \mathcal{E}_N(t)]
$$

$$
\times \theta[-\mathcal{E}_N(t)] - J_j^{2\mathrm{D}}[\mu_j(t), \mu_{j+1}(t), \mathcal{E}_j(t)]\theta[\mathcal{E}_j(t)] + J_j^{2\mathrm{D}}[\mu_j(t), \mu_{j-1}(t), \mathcal{E}_{j-1}(t)]\theta[-\mathcal{E}_{j-1}(t)], \qquad (3)
$$

where the small diffusion current[2,8] is neglected, $\theta(x)$ equals one for $x>0$ and zero for $x\leq 0$, $j=1, 2,\ldots,N$, and $0\leq P_c \leq 1$ is the capture probability of electrons into the QW. P_c depends on the MQW structure parameters and the electric field $\mathcal{E}_b$ across the MQW, and can be calculated through $P_c = [1+B_\infty \exp(-\mathcal{E}_{\mathrm{cp}}/\mathcal{E}_b)]^{-1}$, where B_∞ and $\mathcal{E}_{\mathrm{cp}}$ are the high-field capture coefficient and effective well capturing field determined by the MQW structure.[1] In this article, we will simply take $P_c=0.5$ as an example since it does not change the qualitative features predicted by our model. The first two terms in Eq. (3) represent the forward contributions from capture current into the jth QW, while the third and fourth terms represent the backward contributions from capture cur-

rent into that QW. The last two terms correspond to the forward and backward tunneling currents flowing out of the jth QW.

If electrons in QWs can be approximately viewed as a distribution of sheet charges (zero-thickness), we get the following boundary conditions[2] from the Maxwell equations for two local fields on both sides of the jth QW:

$$
\mathcal{E}_j(t) - \mathcal{E}_{j-1}(t) = \frac{1}{\epsilon_0 \epsilon_r}[\rho_j(t) - en_{2\mathrm{D}}], \qquad (4)
$$

where quantum properties of an electron gas in a QW have been ignored, $n_{2\mathrm{D}}$ is the electron number density in equilibrium, $j=1, 2,\ldots,N$, and ϵ_r is the relative dielectric constant

of the well material. Finally, the sum of individual voltage drops on each period (well plus barrier) is fixed by the voltage $V_b(t)$. This restraint gives rise to

$$L_B\mathcal{E}_0(t)+(L_B+L_W)\sum_{k=1}^{N}\mathcal{E}_k(t)=V_b(t), \qquad (5)$$

and $L_t=L_B+N(L_B+L_W)$ is the total length of the MQW structure in Fig. 1.

Combining Eqs. (3) and (4) for forward contributions we know that the sum of the displacement and conduction currents is a constant for $P_c=1$, i.e.,

$$\epsilon_0\epsilon_r\frac{d\mathcal{E}_{j-1}(t)}{dt}+J_{j-1}^{2D}[\mu_{j-1}(t),\mu_j(t),\mathcal{E}_{j-1}(t)]$$

$$=\epsilon_0\epsilon_r\frac{d\mathcal{E}_j(t)}{dt}+J_j^{2D}[\mu_j(t),\mu_{j+1}(t),\mathcal{E}_j(t)].$$

However, the conduction current itself is not a constant, which creates classical charge-density fluctuations and field domains in MQWs. For non-steady state, the initial condition for Eq. (3) can be set as $\rho_j(0)=en_{2D}$ if the ac electric field is applied to the sample after $t=0$. Equations (3)–(5) together (totally $2N+1$ equations) allow us to simultaneously solve for the charge-density distributions $\rho_k(t)$ [or chemical-potential distributions $\mu_k(t)$] for $k=1, 2,...,N$, as well as for the local-field distributions $\mathcal{E}_k(t)$ for $k=0, 1, 2,...,N$ beyond steady state. For steady state with $d\rho_j(t)/dt=0$, only forward contributions will stay. In this case, we only need to replace Eq. (3) at each moment by[5]

$$J_j^{2D}[\mu_j,\mu_{j+1},\mathcal{E}_j]=P_c J_{inj}^{3D}[\mu_0,\mu_1,\mathcal{E}_0]$$

with $j=1, 2,...,N$. Under this condition, the measured tunneling current density simply equals $J_{inj}^{3D}[\mu_0,\mu_1,\mathcal{E}_0]$. But this does not imply a uniform distribution of charge densities and electric fields.

B. Quantum charge fluctuations

It has been known for a long time that a uniform-field distribution will underestimate or overestimate the sequential-tunneling current in MQWs at high or low voltages, respectively,[5] while the charge density will remain in its equilibrium value even when the uniform electric field is an ac field. In the classical field-domain model,[2,5] quantum properties of electrons in QWs have been ignored. On the other hand, it has also been shown that the quantum nonadiabatic effects give rise to a residual current at zero ac applied voltage due to a space-charge-field effect in the presence of a uniform ac electric field.[3,4,9,10] Therefore it is very important to include, simultaneously, both the classical field-domain effect and the quantum nonadiabatic effect on the sequential tunneling of electrons in MQWs when an ac electric field is applied to the sample.

When the quantum nonadiabatic effect is included, Eq. (3) for $j=1, 2,...,N$ should be modified to

$$\frac{d\rho_j(t)}{dt}=P_c(1-P_c)^{j-1}J_{inj}^{3D}[\mu_0,\mu_1(t),\mathcal{E}_0(t)]\theta[\mathcal{E}_0(t)]+P_c\sum_{k=1}^{j-1}(1-P_c)^{j-k-1}$$

$$\times J_k^{2D}[\mu_k(t)-eL_B\mathcal{E}_k^{na}(t),\mu_{k+1}(t),\mathcal{E}_k'(t)]\theta[\mathcal{E}_k'(t)]-P_c(1-P_c)^{N-j}J_{inj}^{3D}[\mu_0,\mu_N(t),\mathcal{E}_N(t)]\theta[-\mathcal{E}_N(t)]$$

$$-P_c\sum_{k=j+1}^{N}(1-P_c)^{k-j-1}J_k^{2D}[\mu_k(t)-eL_B\mathcal{E}_k^{na}(t),\mu_{k-1}(t),\mathcal{E}_{k-1}'(t)]\theta[-\mathcal{E}_{k-1}'(t)]$$

$$-J_j^{2D}[\mu_j(t)-eL_B\mathcal{E}_j^{na}(t),\mu_{j+1}(t),\mathcal{E}_j'(t)]\theta[\mathcal{E}_j'(t)]$$

$$+J_j^{2D}[\mu_j(t)-eL_B\mathcal{E}_j^{na}(t),\mu_{j-1}(t),\mathcal{E}_{j-1}'(t)]\theta[-\mathcal{E}_{j-1}'(t)]-\left(\frac{L_B}{S}\right)C_{QW}\frac{d\mathcal{E}_j^{na}(t)}{dt}, \qquad (6)$$

where the last term represents the nonadiabatic increase of charge density in the jth QW, $\mathcal{E}_j^{na}(t)$ is the nonadiabatic space-charge field in the jth QW, S is the cross-sectional area of the sample, and $C_{QW}=(m^*e^2S/\pi\hbar^2)f_0[E_0-\mu_e(n_{2D},T)]$ is the quantum capacitance with chemical potential $\mu_e(n_{2D},T)$ for an equilibrium two-dimensional electron gas in QWs. The nonadiabatic space-charge fields $\mathcal{E}_j^{na}(t)$ for $j=1, 2,...,N$ in Eq. (6) are determined by the following differential equations:[4,9,10]

$$C_{QW}\frac{d\mathcal{E}_j^{na}(t)}{dt}=C_{QW}\frac{d\bar{\mathcal{E}}_j(t)}{dt}-\left(\frac{S}{L_B}\right)\Delta J_j^{na}(t), \qquad (7)$$

which contains a "quantum displacement" current due to C_{QW} as a source term. The nonadiabatic change of current density in Eq. (7) is

$$\Delta J_j^{na}(t)$$

$$=J_j^{2D}[\mu_j(t)-eL_B\mathcal{E}_j^{na}(t),\mu_{j+1}(t),\mathcal{E}_j'(t)]\theta[\mathcal{E}_j'(t)]$$

$$-J_j^{2D}[\mu_j(t)-eL_B\mathcal{E}_j^{na}(t),\mu_{j-1}(t),\mathcal{E}_{j-1}'(t)]$$

$$\times\theta[-\mathcal{E}_{j-1}'(t)]-J_j^{2D}[\mu_j(t),\mu_{j+1}(t),\mathcal{E}_j(t)]\theta[\mathcal{E}_j(t)]$$

$$+J_j^{2D}[\mu_j(t),\mu_{j-1}(t),\mathcal{E}_{j-1}(t)]\theta[-\mathcal{E}_{j-1}(t)] \qquad (8)$$

J. Appl. Phys., Vol. 94, No. 6, 15 September 2003

D. Huang and D. A. Cardimona   3707

with $\mathcal{E}_{N+1}^{na}(t)=0$. The charge-density fluctuations in Eq. (6) now contain both adiabatic and nonadiabatic contributions given by the last term in Eq. (6). The total field $\mathcal{E}_k'(t)$ and the average field $\bar{\mathcal{E}}_j(t)$ in Eqs. (6) and (7) are defined by

$$\begin{bmatrix} \mathcal{E}_k'(t) \\ \bar{\mathcal{E}}_k(t) \end{bmatrix} = \begin{bmatrix} \mathcal{E}_k(t)+\mathcal{E}_k^{na}(t) \\ [\mathcal{E}_k(t)+\mathcal{E}_{k-1}(t)]/2 \end{bmatrix}.$$

Simultaneously, Eq. (4) should also be modified to

$$\mathcal{E}_j(t)-\mathcal{E}_{j-1}(t)-\left(\frac{C_{QW}}{C_0}\right)\mathcal{E}_j^{na}(t)=\frac{1}{\epsilon_0\epsilon_r}[\rho_j(t)-en_{2D}], \tag{9}$$

where $C_0=\epsilon_0\epsilon_r S/L_B$ is the classical geometric capacitance. For non-steady state, the total measured current density for $V_b(t)\geqslant 0$ is given by

$$\begin{aligned} J_m^{ns(+)}(t)=&(1-P_c)^N J_{inj}^{3D}[\mu_0,\mu_1(t),\mathcal{E}_0(t)]\theta[\mathcal{E}_0(t)] \\ &+\sum_{k=1}^{N} (1-P_c)^{N-k} \\ &\times J_k^{2D}[\mu_k(t)-eL_B\mathcal{E}_k^{na}(t),\mu_{k+1}(t),\mathcal{E}_k'(t)] \\ &\times\theta[\mathcal{E}_k'(t)]+J_{inj}^{3D}[\mu_0,\mu_N(t),\mathcal{E}_N(t)]\theta[-\mathcal{E}_N(t)] \\ &+\left(\frac{L_B C_0}{S}\right)\frac{d\mathcal{E}_N(t)}{dt}, \end{aligned} \tag{10}$$

which includes both conduction and dielectric displacement currents, where the last term represents the displacement current from the geometric capacitance. In this case, the in-flowing injection current is not equal to the out-flowing conduction current from the sample due to $d\rho_j(t)/dt\neq 0$. On the other hand, for $V_b(t)<0$ we have

$$\begin{aligned} J_m^{ns(-)}(t)=&(1-P_c)^N J_{inj}^{3D}[\mu_0,\mu_N(t),\mathcal{E}_N(t)]\theta[-\mathcal{E}_N(t)] \\ &+\sum_{k=1}^{N} (1-P_c)^{k-1} \\ &\times J_k^{2D}[\mu_k(t)-eL_B\mathcal{E}_k^{na}(t),\mu_{k-1}(t),\mathcal{E}_{k-1}'(t)] \\ &\times\theta[-\mathcal{E}_{k-1}'(t)]+J_{inj}^{3D}[\mu_0,\mu_1(t),\mathcal{E}_0(t)]\theta[\mathcal{E}_0(t)] \\ &+\left(\frac{L_B C_0}{S}\right)\frac{d\mathcal{E}_0(t)}{dt}. \end{aligned} \tag{11}$$

In steady state, however, there is no nonadiabatic charge-density fluctuation, and the total measured current density is mainly determined by the injection current, which is given for $V_b(t)\geqslant 0$ by

$$J_m^s(t)=J_{inj}^{3D}[\mu_0,\mu_1(t),\mathcal{E}_0(t)]+\left(\frac{L_B C_0}{S}\right)\frac{d\mathcal{E}_N(t)}{dt}, \tag{12}$$

which can be modified by the local field at the emitter barrier. Moreover, due to $d\rho_j(t)/dt\neq 0$ in non-steady state we can define a total effective differential capacitance for the MQW structure

$$C_{di}(t)\equiv\sum_{j=1}^{N} C_{di}^j(t)=\left[\frac{dV_b(t)}{dt}\right]^{-1}S\sum_{j=1}^{N}\frac{d\rho_j(t)}{dt}, \tag{13}$$

which is time-dependent and different from both C_0 and C_{QW}.

From Eq. (9) we know that both the field-domain and nonadiabatic effects will cause charge density fluctuations in QWs in the presence of an ac electric field. The quantum capacitance C_{QW} only enters into Eq. (6) for the charge-density fluctuations but not into Eq. (10) for the total measured current density $J_m^{ns(\pm)}(t)$. Instead, the conduction current is modified by the nonadiabatic space-charge field $\mathcal{E}_{na}(t)$ which is induced by the "quantum displacement" current as shown in Eq. (7). On the other hand, the geometric capacitance C_0 directly modifies the total measured current in Eq. (10) as a contribution from the dielectric displacement current but does not enter into the charge fluctuations in Eq. (6). When only the forward contributions are included, the sum of dielectric displacement and conduction currents flowing into and out of a QW is a constant for $P_c=1$. Because the conduction current flowing into the first QW is simply the injection current from the contact layer, the change in the conduction currents flowing into different QWs is determined by the variation of the dielectric displacement currents due to the nonuniform electric-field distribution inside the whole system. From Eq. (7) we further find that even under a uniform ac electric field, the nonadiabatic conduction current density flowing through each QW is not equal to the sum of adiabatic sequential-tunneling current flowing out of the QW and the "quantum displacement" current density $L_B C_{QW}d\bar{\mathcal{E}}_j(t)/dt$ because $d\mathcal{E}_j^{na}(t)/dt\neq 0$. If the nonadiabatic effect [or $\mathcal{E}_j^{na}(t)$] is small and the backward contributions are neglected, Eq. (6) can be expanded to leading order as

$$\begin{aligned} \frac{d\rho_j(t)}{dt}\approx & P_c\sum_{k=1}^{j-1} (1-P_c)^{j-k-1}J_k^{2D}[\mu_k(t),\mu_{k+1}(t),\mathcal{E}_k(t)] \\ &+P_c(1-P_c)^{j-1}J_{inj}^{3D}[\mu_0,\mu_1(t),\mathcal{E}_0(t)] \\ &-J_j^{2D}[\mu_j(t),\mu_{j+1}(t),\mathcal{E}_j(t)] \\ &-\left(\frac{L_B}{S}\right)C_{QW}\frac{d\bar{\mathcal{E}}_j(t)}{dt}+\left(\frac{L_B}{S}\right)P_c\sum_{k=1}^{j-1} (1-P_c)^{j-k-1} \\ &\times\left\{\frac{\mathcal{E}_k^{na}(t)}{\mathcal{R}_k'[\mu_k(t),\mu_{k+1}(t),\mathcal{E}_k(t)]}\right\}, \end{aligned} \tag{14}$$

where the differential resistance in Eq. (14) is defined by

$$\frac{1}{\mathcal{R}_k'[\mu_k(t),\mu_{k+1}(t),\mathcal{E}_k(t)]}=\left(\frac{S}{L_B}\right)\left\{\frac{\partial}{\partial\mathcal{E}_k}J_k^{2D}[\mu_k(t),\mu_{k+1}(t),\mathcal{E}_k(t)]\right\}.$$

The first three terms in Eq. (14) represent the contributions from field domains. The last two terms come from the main quantum nonadiabatic contributions. The other small nonadiabatic terms associated with the relative change in charge
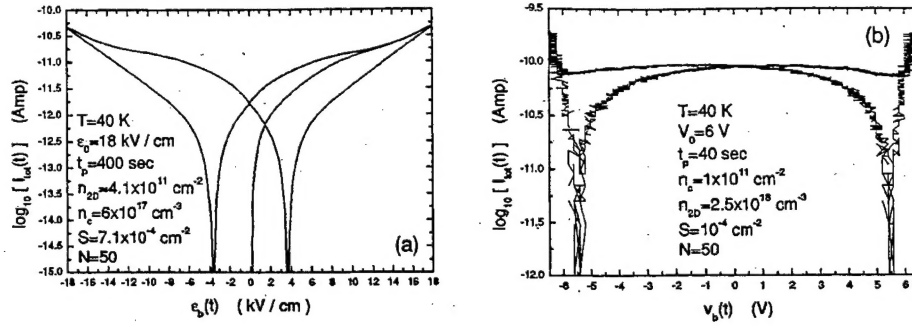
FIG. 2. Comparison of results for total tunneling current $I_{tot}(t)$ in a logarithm scale as a function of the applied sinusoidal bias from theory [in (a)] and experiment [in (b)] using $I_{tot}(t) = S[J^{2D}(t) + \Delta J^{na}(t)]$. Here, barrier material is $Al_{0.3}Ga_{0.7}As$ and well material is GaAs, $L_W = 50$ Å, $N = 50$, and $T = 40$ K. For numerical calculation, we set $n_c = 6 \times 10^{17}$ cm^{-3}, $n_{2D} = 4.1 \times 10^{11}$ cm^{-2}, $t_p = 400$ s, $S = 7.1 \times 10^{-4}$ cm^{-2}, and $\mathcal{E}_0 = 18$ kV/cm. The parameters used in the experiment are $n_c = 1 \times 10^{18}$ cm^{-3}, $n_{2D} = 2.5 \times 10^{11}$ cm^{-2}, $t_p = 40$ s, $S = 1 \times 10^{-4}$ cm^{-2}, $V_0 = \mathcal{E}_0 L_t = 6$ V, and $V_0 = \mathcal{E}_0 L_t$.

densities between neighboring QWs are neglected in Eq. (14). Similarly, Eq. (7) can also be expanded to leading order as

$$\frac{d\mathcal{E}_j^{na}(t)}{dt} \approx \frac{d\bar{\mathcal{E}}_j(t)}{dt} - \left\{ \frac{\mathcal{E}_j^{na}(t)}{\mathcal{R}_j'[\mu_j(t),\mu_{j+1}(t),\mathcal{E}_j(t)]C_{QW}} \right\}, \quad (15)$$

which reduces to the previous result[4,9,10] for the case of a uniform ac electric field.

III. NUMERICAL RESULTS AND DISCUSSIONS

In this section, we present numerical results for distributions of both local fields and charge densities in a MQW sample. We first concentrate on effects of classical charge fluctuations described by Eqs. (3)–(5) for non-steady state. After this, effects of quantum charge fluctuations will be addressed based on Eqs. (5)–(9).

The sample we consider in this article is an AlGaAs/GaAs MQW structure. The total number of QWs is $N = 10$, with 11 barriers. The parameters for this sample are: well thickness $L_W = 75$ Å, barrier thickness $L_B = 339$ Å, barrier height $V_0 = 224.5$ MeV, electron effective mass $m^* = 0.065\, m_0$ with free electron mass m_0, electron areal density $n_{2D} = 5 \times 10^{11}$ cm^{-2}, contact-layer electron concentration $n_c = 6 \times 10^{17}$ cm^{-3}, cross-sectional area $S = 10^{-4}$ cm^2, capture probability $P_c = 0.5$, saturation velocity $v_s = 2 \times 10^6$ cm/s, saturation field $\mathcal{E}_s = 2$ kV/cm, and relative dielectric constant $\epsilon_r = 12$. The ground-state subband edge is

calculated to be $E_0 = 44.1$ MeV. The voltage is defined to be $V_b(t) = \mathcal{E}_{ac}(t)L_t$ with $\mathcal{E}_{ac}(t) = \mathcal{E}_0 \sin(2\pi t/t_p)$ for $t \geqslant 0$, where the field amplitude $\mathcal{E}_0 = 5$ kV/cm and the time period $t_p = 0.1$ s. The changes in the sample parameters for the numerical calculations will be indicated in the figure captions. [For typical MQW photodetectors, the ground and excited states are designed to be bound and quasi-bound, respectively. However, for $V_0 = 224.5$ meV the choice of $L_W = 75$ Å and $L_B = 339$ Å leads to two lowest bound states in QW. Since we only study in this article the effects of classical and quantum charge fluctuations on the dark current, the selection of excited state does not change the qualitative features predicted by our model.]

We first show in Fig. 2(a) a comparison between the experimental data and the theoretical result from our generalized model in Eqs. (5)–(9) at $T = 40$ K. This comparison highlights the importance and uniqueness of the nonadiabatic tunneling effect included in our generalized model. From Fig. 2(b) we clearly observe a nonzero residual current from the experiment when the ac voltage is swept through zero. This phenomenon cannot be understood at all by Levine's adiabatic tunneling model[1] which has been widely applied to study dark current in quantum-well photodetectors. However, the nonzero residual current observed experimentally has been successfully reproduced and explained by $\mathcal{E}_k^{na}(t) \neq 0$ due to the nonadiabatic tunneling effect which is the spirit of our generalized model presented in Eqs. (5)–(9) of this article.
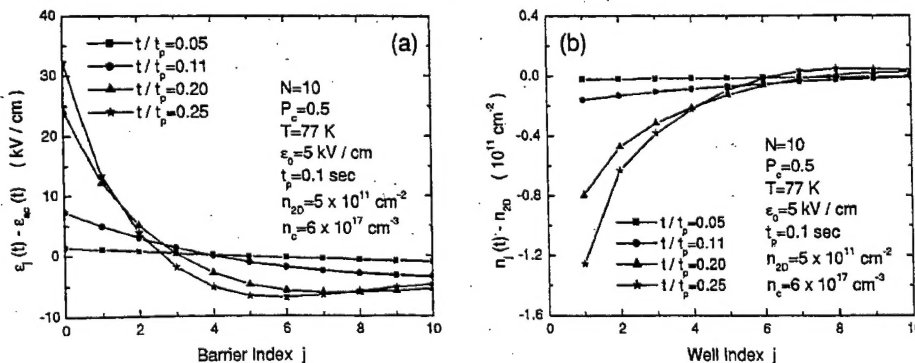

FIG. 3. Calculated local fields $\mathcal{E}_j(t) - \mathcal{E}_{ac}(t)$ in (a) in different barrier layers and density fluctuations $n_j(t) - n_{2D}$ in (b) inside different QWs at times $t/t_p = 0.05$, 0.11, 0.20, and 0.25 s.
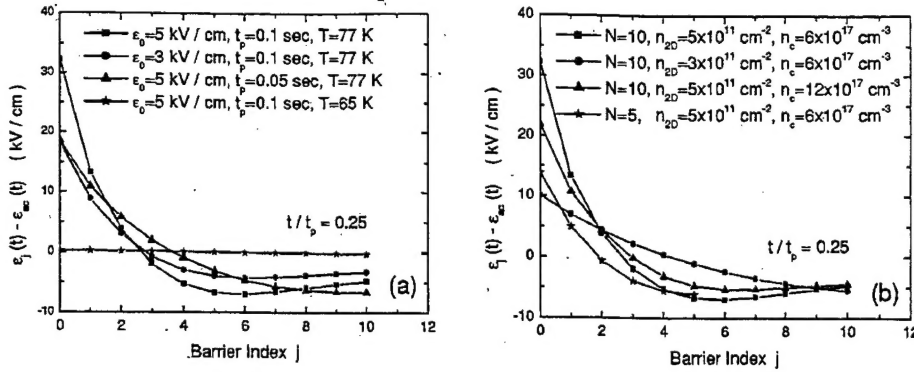
FIG. 4. Calculated local fields $\mathcal{E}_j(t) - \mathcal{E}_{ac}(t)$ in different barrier layers at the time $t/t_p = 0.25$ s. Here, the comparison of $\mathcal{E}_j(t) - \mathcal{E}_{ac}(t)$ with different values of $\mathcal{E}_0$, t_p, and T are presented in (a) and the comparison of those with different values of N, n_{2D}, and n_c are shown in (b). The changed parameters are indicated. The other parameters used in calculations are the same as those in Fig. 3.

A. Effects of classical charge fluctuations

We show in Fig. 3 the local fields $\mathcal{E}_j(t) - \mathcal{E}_{ac}(t)$ in different layers [in (a)] and the density fluctuation $n_j(t) - n_{2D}$ in different QWs [in (b)] at several times t/t_p for $T = 77$ K. From (a) we find that the field-domain effect is negligible at $t/t_p = 0.05$ (very small applied field) because both the injection current J_{inj}^{3D} and the sequential-tunneling current J_k^{2D} are both extremely small in this case. With the increase of $\mathcal{E}_{ac}(t)$, i.e., t/t_p increases from 0.05 to 0.25, fields close to the emitter barrier are enhanced dramatically relative to the uniform field $\mathcal{E}_{ac}(t)$. This is a result of the huge current imbalance $J_{inj}^{3D} \ll J_1^{2D}$ under the uniform field $\mathcal{E}_{ac}(t)$, as explained in Fig. 1(b). At the same time, fields close to the receiver barrier are suppressed almost to zero. From Fig. 3(b) we find that when $\mathcal{E}_{ac}(t)$ is large, densities close to the emitter barrier are greatly reduced with respect to the equilibrium value n_{2D}. This is accompanied by a great enhancement of the local field $\mathcal{E}_0(t) \gg \mathcal{E}_{ac}(t)$ at the emitter barrier, as shown in Fig. 3(a). However, densities close to the receiver barrier remain near to n_{2D} due to the suppressed local field $\mathcal{E}_N(t) \approx 0$. It is obvious from Fig. 3(b) that some electrons have been removed from the sample since $\Sigma_j[n_j(t) - n_{2D}] < 0$, which is true even for steady state. The calculation done here corresponds to a non-steady state. Therefore the net number of electrons removed from the sample changes with time under an ac voltage, leading to a differential capacitance $C_{di}^j(t)$ [see Eq. (13)].

Figure 4 compares local fields $\mathcal{E}_j(t) - \mathcal{E}_{ac}(t)$ at $t/t_p = 0.25$ as a function of barrier index j for different values of $\mathcal{E}_0$, t_p, T in (a) and different values of N, n_{2D}, n_c in (b). From Fig. 4(a) we find that the field-domain effect is negli-

gible at $T \leqslant 65$ K due to very small injection and sequential-tunneling currents at these temperatures. The bigger the field amplitude $\mathcal{E}_0$ is, the larger $\mathcal{E}_0(t)$ will be. A smaller t_p leads to a negative $\mathcal{E}_N(t)$ on the receiver barrier due to the strong nonsteady effect. This is completely different from the steady-state results in Refs. 1 and 5 in which $\mathcal{E}_N(t)$ will always be positive. Furthermore, we find from Fig. 4(b) that the smaller the number of QWs N is, the lower $\mathcal{E}_0(t)$ is. The increase of n_{2D} causes a larger sequential-tunneling current, leading to a larger value of $\mathcal{E}_0(t)$ due to an enhanced current imbalance between J_{inj}^{3D} and J_1^{2D}. Conversely, the increase of n_c introduces a bigger injection current, leading to a smaller value of $\mathcal{E}_0(t)$ due to a suppressed current imbalance between J_{inj}^{3D} and J_1^{2D}.

Figure 5 presents density fluctuations $n_j(t) - n_{2D}$ as a function of well index j at the moment of maximum $\mathcal{E}_{ac}(t)$ for different values of $\mathcal{E}_0$, t_p, T in (a) and different values of N, n_{2D}, n_c in (b). Corresponding to Fig. 4(a), Fig. 5(a) shows a stronger charge depletion in the first QW when temperature T is higher or field amplitude $\mathcal{E}_0$ is larger. Accompanying Fig. 4(b), Fig. 5(b) also exhibits a larger deviation of $n_1(t)$ away from n_{2D} for a smaller value of n_c or bigger values of N and n_{2D}.

As we know from Eq. (5), the field-domain distribution depends on $V_b(t) = \mathcal{E}_{ac}(t)L_t$ at each moment t. Different times imply different values of local field $\mathcal{E}_j(t)$ within the jth barrier layer or different values of density $n_j(t)$ inside the jth QW. However, $dn_j(t)/dt = 0$ for each moment in steady state. In non-steady state, we can define a differential capacitance as in Eq. (13), which is proportional to $dn_j(t)/dt \neq 0$. The calculated results for $C_{di}(t)$ are shown in Fig. 6(b) for
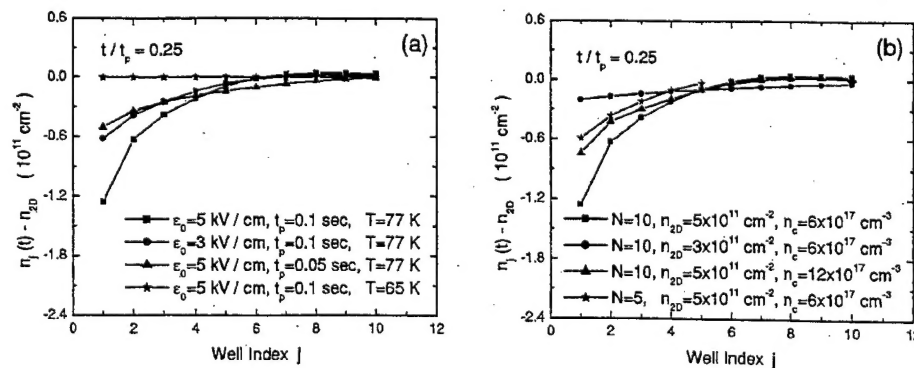

FIG. 5. Calculated density fluctuations $n_j(t) - n_{2D}$ inside different QWs at the time $t/t_p = 0.25$ s. Here the comparison of $n_j(t) - n_{2D}$ with different values of $\mathcal{E}_0$, t_p, and T are presented in (a) and the comparison of those with different values of N, n_{2D}, and n_c are shown in (b). The changed parameters are indicated in figures. The other parameters used in calculations are the same as those in Fig. 3.
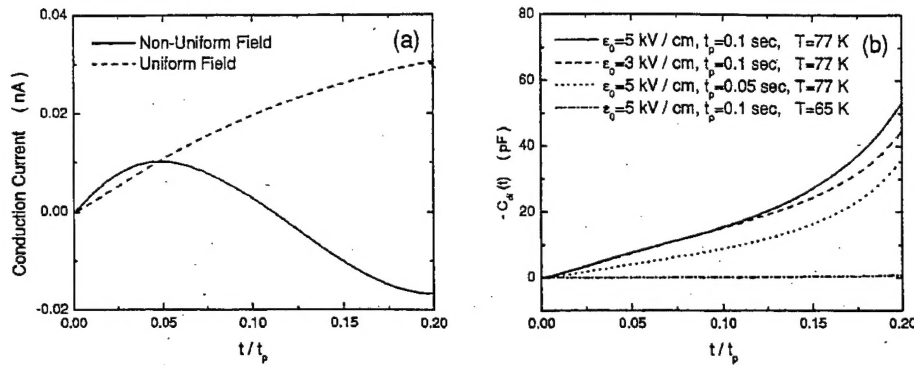
FIG. 6. Effective total differential capacitance $C_{di}(t)$ in (a) and comparisons of conduction currents in (b) for non-steady state with nonuniform and uniform electric fields and different values of $\mathcal{E}_0$, t_p, and T. The conduction current is calculated by setting $\mathcal{E}_j^{na}(t) = 0$, and the adiabatic $C_{di}(t)$ is also calculated with $\mathcal{E}_j^{na}(t) = 0$. The changed parameters are indicated in figures. The other parameters used in calculations are the same as those in Fig. 3.

different values of $\mathcal{E}_0$, t_p, and T. It is clear from (b) that $C_{di}(t)$ is always negative, increases greatly with $\mathcal{E}_{ac}(t)$, and becomes nearly zero at $T \leqslant 65$ K. The value of $C_{di}(t)$ is dominated by $C_{di}^1(t)$ in the first QW. Whenever $|n_1(t) - n_{2D}|$ is larger in Fig. 5(a), $-C_{di}(t)$ becomes bigger in Fig. 6(b). From an experimental point of view, the conduction current detected by the receiver, as described by Eq. (14) without the last term, is of great interest. We show in Fig. 6(a) the conduction current as a function of time t/t_p. In order to see the effects of classical charge fluctuations, we compare the conduction current calculated from Eq. (14) by excluding the last term and setting $\mathcal{E}_j^{na}(t) = 0$ (solid curve) with the current calculated from Eq. (2) by setting $\mathcal{E}_k(t) = \mathcal{E}_{ac}(t)$ for a uniform electric field and $n_k(t) = n_{2D}$ (dashed curve). When $\mathcal{E}_{ac}(t)$ is small with $t/t_p \leqslant 0.05$, solid and dashed curves agree very well due to $\mathcal{E}_N(t) \approx \mathcal{E}_{ac}(t)$ as seen from Fig. 3(a). However, the solid curve falls below the dashed curve after $t/t_p = 0.05$ and then changes sign when $t/t_p > 0.1$. The solid curve in (a) can qualitatively be explained by Fig. 3(a), where with the increase of t/t_p, $\mathcal{E}_N(t)$ starts at $\mathcal{E}_{ac}(t)$, and then becomes negative, and finally approaches zero. The negative conduction current observed in (a) is a direct result of our non-steady-state conditions, which is completely different from those in Refs. 1 and 5 for steady state.

To summarize the above observations, effects of classical charge fluctuations only play a role under the condition of a large imbalance between the injection and sequential-tunneling currents near the emitter barrier. This can be achieved by increasing either the temperature T or the field amplitude $\mathcal{E}_0$.

B. Effects of quantum charge fluctuations

Effects of classical charge fluctuations depend on the geometric capacitance C_0, as shown by Eq. (4). However, the quantum capacitance C_{QW} starts to play a role when the nonadiabatic effect is included, as seen from Eq. (9). The striking thing is that the effects of quantum charge fluctuations become more and more important as $T \leqslant 65$ K, while the effects of classical charge fluctuations are negligible at these temperatures. We compare in Fig. 7 two calculated nonadiabatic fields $\mathcal{E}_j^{na}(t)$ at $t/t_p = 0.25$ as a function of well index j for $T = 40$ and 77 K. From the figure we know that $\mathcal{E}_j^{na}(t)$ decreases with j due to field-domain effects at T

$= 77$ K. However, $\mathcal{E}_j^{na}(t)$ becomes independent of j at $T = 40$ K. More importantly, $\mathcal{E}_j^{na}(t)$ increases with reducing T.

The effect of nonadiabatic field $\mathcal{E}_j^{na}(t)$ can be seen more clearly from the calculated local fields $\mathcal{E}_j(t) - \mathcal{E}_{ac}(t)$ in different barrier layers in Fig. 8(a) and density fluctuations $n_j(t) - n_{2D}$ in different QWs in Fig. 8(b) at $t/t_p = 0.25$ with various values of $\mathcal{E}_0$, t_p, and T. By comparing solid and dashed curves in (a) we find that $\mathcal{E}_0(t)$ is reduced by a factor of 2 as $\mathcal{E}_0 = 5$ kV/cm, $t_p = 0.1$ s, and $T = 77$ K (squares). Moreover, $\mathcal{E}_0(t)$ decreases even more due to $\mathcal{E}_j^{na}(t)$ when t_p is reduced to 0.05 s (stars) due to stronger nonsteady effects, but it decreases much less when T is reduced to 40 K (triangles) due to smaller injection and sequential-tunneling currents. However, $\mathcal{E}_0(t)$ is enhanced by nonadiabatic effects when $\mathcal{E}_0$ is reduced to 1 kV/cm (circles). All of these features have a strong influence on $C_{di}^1(t)$, as discussed in Fig. 6(a). On the other hand, from (a) we also find that $\mathcal{E}_N(t)$ becomes a much more negative value for $\mathcal{E}_0 = 5$ kV/cm, $t_p = 0.1$ s, and $T = 77$ K when $\mathcal{E}_j^{na}(t)$ is included in our calculations (solid curve with squares) than when it is excluded (dashed curve with squares). The same situation occurs when either t_p is reduced to 0.05 s (stars) or $\mathcal{E}_0$ is reduced to 1 kV/cm (circles) but with a smaller overall magnitude compared to the curves with the squares. As explained in Fig. 6(b), the features observed for $\mathcal{E}_N(t)$ in Fig. 8(a) will affect the conduction cur-
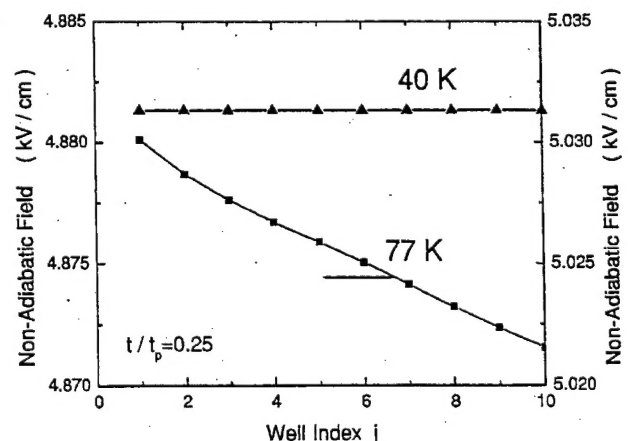

FIG. 7. Calculated nonadiabatic space-charge fields $\mathcal{E}_j^{na}(t)$ at $t/t_p = 0.25$ as a function of well index j for $T = 40$ and 77 K (left scaled), respectively. The other parameters used in calculations are the same as those in Fig. 3.
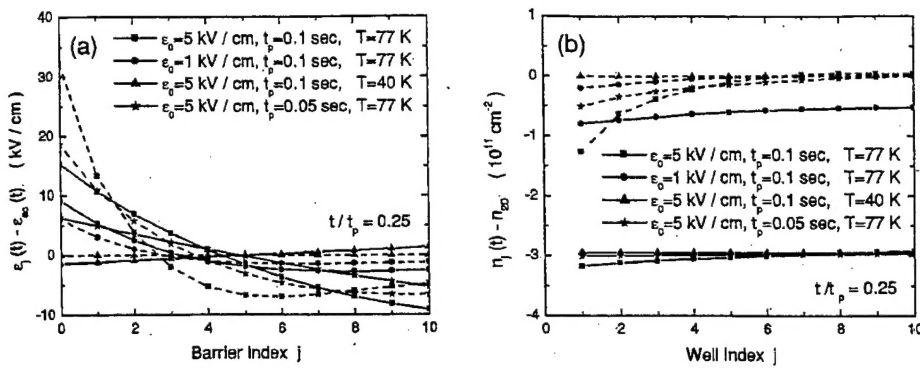
FIG. 8. Calculated local fields $\mathcal{E}_j(t) - \mathcal{E}_{ac}(t)$ in different barrier layers and density fluctuations $n_j(t) - n_{2D}$ inside different QWs at $t/t_p = 0.25$ with different values of $\mathcal{E}_0$ (black/red curves), t_p (black/blue curves), and T (black/green curves). $\mathcal{E}_j(t) - \mathcal{E}_{ac}(t)$ are compared in (a) with (solid curves) and without (dashed curves) $\mathcal{E}_j^{na}(t)$, and the similar comparisons of $n_j(t) - n_{2D}$ are presented in (b). The changed parameters are indicated in figures. The other parameters used in calculations are the same as those in Fig. 3.

rent detected at the receiver layer. Effects of quantum charge fluctuations are reflected in the calculated $n_j(t) - n_{2D}$ in (b), where the reduction of charge in the QWs is greatly increased except for the case with a small value of $\mathcal{E}_0$ (circles). Although there is a strong dependence of $\mathcal{E}_j(t)$ on index j near the emitter barrier, there is very little dependence of $n_j(t)$ on j there after $\mathcal{E}_j^{na}(t)$ is included in the calculations.

IV. CONCLUSIONS

In conclusion, by including nonadiabatic space-charge-field effects we have generalized the previous theories for studying field-domain effects in MQW photodetectors in the presence of an ac voltage. We have found from our numerical calculations that field-domain effects are only important at high temperatures or high voltages, which implies the existence of significant injection and sequential-tunneling currents in the system. We have further found that nonadiabatic effects become much more visible at low temperatures and low voltages when the field-domain effects are negligible. The time duration for nonadiabatic effects has been found to relate to the quantum capacitance, while the dielectric displacement current has been shown to be controlled by the geometrical capacitance. For non-steady state, we have found a negative differential capacitance in the system, and we have predicted a negative conduction current under a positive voltage.

In this article, we have assumed that the capture probability is independent of electric field. This can be justified by the fact that the capture probability is near a constant at low electric fields. In the presence of incident photons, the conduction current flowing through the MQW sample will be the sum of sequential-tunneling and photoexcited currents. From our studies in this article, we predict that the field domain effects which are significant at high temperatures or high photon fluxes will strongly affect both tunneling- and photo-currents. On the other hand, nonadiabatic effects modify these currents at low temperatures and low photon

fluxes when the current flowing through MQWs is large. These latter conditions are of utmost importance in any space-based detector applications.

One of the main results of this work is the prediction of the dominance of field-domain effects at 77 K and above and the dominance of nonadiabatic effects at 40 K and below. The experimental observation of anomalous nonadiabatic behavior in sequential-tunneling current at low temperatures and the suppression of it at high temperatures has already been demonstrated.[2,3] For a bound-to-bound multiple-quantum-well photodetector, if there exists only one negative-differential-conductance peak at a voltage predicted by a uniform-field model at low temperatures, it is an indication of the suppression of the field-domain effect.[11]

ACKNOWLEDGMENT

[1] B. F. Levine, J. Appl. Phys. **74**, R1 (1993).
[2] M. Ershov, V. Ryzhii, and C. Hamaguchi, Appl. Phys. Lett. **67**, 3147 (1995).
[3] A. Singh and D. A. Cardimona, Opt. Eng. **38**, 1424 (1999).
[4] D. H. Huang, A. Singh, and D. A. Cardimona, J. Appl. Phys. **87**, 2427 (2000).
[5] L. Thibaudeau, P. Bois, and J. Y. Duboz, J. Appl. Phys. **79**, 446 (1996).
[6] D. H. Huang, A. Singh, and D. A. Cardimona, Phys. Lett. A **259**, 488 (1999).
[7] D. H. Huang and D. A. Cardimona, Phys. Rev. B **67**, 245306 (2003).
[8] R. Aguado, G. Platero, M. Moscoso, and L. Bonilla, Phys. Rev. B **55**, R16053 (1997).
[9] D. H. Huang, C. Morath, D. A. Cardimona, and A. Singh, J. Appl. Phys. **90**, 6032 (2001).
[10] D. H. Huang, A. Singh, D. A. Cardimona, and C. Morath, J. Appl. Phys. **89**, 4429 (2001).
[11] Some preliminary experimental results from our research group on the measurement of differential resistance for the dark current flowing inside multiple-quantum-well photodetectors have indicated that the field-domain effect has been suppressed at low temperatures, seen as a single maximum in the curves of resistance vs applied voltage.